WDM-Coherent OCDMA over one single device based on short chip Super structured fiber Bragg gratings

Waldimar Amaya*, Daniel Pastor, Rocio Baños, and Victor Garcia-Munoz

Institute of Telecommunications and Multimedia Applications (iTEAM), Universidad Politécnica de Valencia, Camino de Vera S/N, 46021 Valencia- Spain
**walamoc@iteam.upv.es*

Abstract: We theoretically propose and demonstrate experimentally a Coherent Direct Sequence OCDMA en/decoder for multi-channel WDM operation based on a single device. It presents a broadband spectral envelope and a periodic spectral pattern that can be employed for en/decoding multiple sub-bands simultaneously. Multi-channel operation is verified experimentally by means of Multi-Band Super Structured Fiber Bragg Gratings with binary phase encoded chips fabricated with 1mm inter-chip separation that provides 4x100 GHz ITU sub-band separation at 1.25 Gbps. The WDM-OCDMA system verification was carried out employing simultaneous encoding of four adjacent sub-bands and two different OCDMA codes.

OCIS codes: (060.0060) Fiber optics and optical communications; (060.3735) Fiber Bragg gratings; (230.0230) Optical devices.

References and links

1. P. Green, "Paving the last mile with glass," IEEE Spectr. **39**(12), 13–14 (2002).
2. K. Kitayama, X. Wang, and N. Wada, "OCDMA over WDM PON-solution path to gigabit-symmetric FTTH," J. Lightwave Technol. **24**(4), 1654–1662 (2006).
3. X. Wang, K. Matsushima, A. Nishiki, N. Wada, F. Kubota, and K.-I. Kitayama, "Experimental demonstration of 511-chip 640 Gchip/s superstructured FBG for high performance optical code processing," in *Proc. of the Europeam Conference Optical Communication (ECOC)*, (Stockholm, Sweden, 2004), Paper Tu1.3.7.
4. W. Amaya, D. Pastor, and J. Capmany, "Modeling of a Time-Spreading OCDMA System Including Nonperfect Time Gating, Optical Thresholding, and Fully Asynchronous Signal/Interference Overlapping," J. Lightwave Technol. **26**(7), 768–776 (2008).
5. X. Wang and N. Wada, "Experimental Demonstration of OCDMA Traffic Over Optical Packet Switching Network With Hybrid PLC and SSFBG En/Decoders," J. Lightwave Technol. **24**(8), 3012–3020 (2006).
6. K. Matsushima, X. Wang, S. Kutsuzawa, A. Nishiki, S. Oshiba, N. Wada, and K. Kitayama, "Experimental demonstration of performance improvement of 127-chip SSFBG en/decoder using apodization technique," IEEE Photon. Technol. Lett. **16**(9), 2192–2194 (2004).
7. P. C. Teh, M. Ibsen, J. H. Lee, P. Petropoulos, and D. J. Richardson, "Demonstration of a Four-Channel WDM/OCDMA System Using 255-Chip 320-Gchip/s Quaternary Phase Coding Gratings," IEEE Photon. Technol. Lett. **14**(2), 227–229 (2002).
8. H. Zheng, B. Chen, D. Wang, X. Hong, and S. He, "Investigation of DWDM over OCDMA System Based on Parallelly Combined SSFBG Encoder/Decoders," in *Proceedings of Symposium on Photonics and Optoelectronics (SOPO),* (Wuhan, China, 2011), 1–3.
9. M. Abramowitz and I. A. Stegun, *Handbook of Mathematical Functions with Formulas, Graphs, and Mathematical Tables*, (New York: Dover Publications, 1972).
10. D. Pastor, W. Amaya, and R. Garcia-Olcina, "Coherent Direct Sequence optical en/decoding employing low cost DFB lasers with narrow optical band consumption – towards realizable photonic label switching," in *Proceedings of 12th International Conference on Transparent Optical Networks (ICTON)*,(Munich, Germany, 2010), 1–4.
11. D. Pastor, W. Amaya, R. García-Olcina, and S. Sales, "Coherent direct sequence optical code multiple access encoding-decoding efficiency versus wavelength detuning," Opt. Lett. **32**(13), 1896–1898 (2007).

1. Introduction

In the last years, fiber to the home *(FTTH)* has been proposed as a solution for the last mile bottleneck in metropolitan networks for residential and business users. FTTH can be

#155203 - $15.00 USD Received 22 Sep 2011; revised 21 Oct 2011; accepted 28 Oct 2011; published 16 Nov 2011

implemented over passive optical networks (PON) with negligible impact. From the viewpoint of service provider it requires small changes in its infrastructure and from the perspective of end user it represents the possibility of having better and more services (HDTV, high speed Internet, IP telephony, etc) [1]. For the implementation of FTTH three techniques have been proposed: Optical Time Division Multiplexing (OTDM), Wavelength Division Multiplexing (WDM) and more recently Optical Code Division Multiple Access (OCDMA). Although OTDM and WDM have important advantages, they present some drawbacks. The OTDM uplink rate is limited because all the users share the same bandwidth. On the other hand, WDM is limited in number of channels [2]. OCDMA is an emergent technology limited until now for the immaturity of optical devices, however recently a great progress has been observed in the en/decoder devices and time gating techniques [3] that makes OCDMA a good alternative for multiple access solution in FTTH implementations. In particular, the Coherent Direct Sequence (CDS) OCDMA technique has been demonstrated employing different technologies as en/decoder devices such as planar lightwave circuits and superstructured fiber Bragg gratings (SSFBG) and applied for multiple user access networks [4–7]. Standard single channel CDS technique consists in: 1) one optical pulse is applied to the encoder which must provide N copies of it, called chips, along the time axis separated by the inter-chip time tch. 2) Each chip (or individual part of the encoded signal) has the encoding information in amplitude or phase accordingly to a given code word. 3) At the decoder front end, the process is reversed to provide a proper Auto-Correlation Peak (ACP) (desired signal) or a Cross-Correlation (XC) signal between undesired interference users.

One main advantage of the CDS-OCDMA technique is that it can be exploited in combination with WDM signals or conveyed into WDM bands as has been previously proposed by several authors [2, 7, 8]. In [2] a Coarse WDM/OCDMA system is proposed employing codes with 511 chips and 10 nm width-channel, this approach implies 5 nm channel separation and thus is hardly applicable with 100 GHz WDM separation. The group of Petropoulos [7] proposed a WDM/OCDMA system which employed one different en/decoding device based on standard SSFBGs for each channel. This approach can lead to complex and cumbersome systems, with the main inconvenience that all the SSFBGs have to be stabilized in temperature independently. Another DWDM-OCDMA system is proposed by simulations in [8], in this case a single device can encode three adjacent 100 GHz WDM channels; but as we will demonstrate, the proposed schema presents coding capacity losses.

In this paper we propose and demonstrate a single device that provides a real WDM-OCDMA system without coding capacity loss. This device is based on short time chips compared with its inter-chip time separation and can be employed for en/decoding of multiple sub-bands simultaneously exploiting the total capacity of the code. We will theoretically demonstrate with averaging results over a family of 32 codes from the Gold-63 family the possibility of encode the same code over several adjacent channels. For the experimental verification we fabricated the proposed Multiple-channel Super Structured Fiber Bragg Gratings with $N = 63$ chips encoded in binary phase with 1mm inter-chip separation that provides 100 GHz ITU sub-band channeling. The final en/decoding device presents up to 4x100GHz sub-bands with an insertion loss penalty between 3 and 4 dB from centre to lateral bands.

2. Multi-band SSFBG proposal

As said before, in the CDS-OCDMA scheme, the encoder structure produces N copies of the original pulse. Thus, the impulse response for the CDS device under low reflectivity regime used for code *"p"* can be expressed as

$$h_p^{en}(t) = h_{chip}(t) \otimes \sum_{k=1}^{N} a_{p,k}^{en} \exp(j\phi_{p,k}^{en}) \delta(t - kt_{ch}) \tag{1}$$

where $h_{chip}(t)$ is the individual chip impulse response given by the technology or the fabrications limitations, $a_{p,k}^{en}$ and $\phi_{p,k}^{en}$ are the amplitude and phase imposed by the code word

#155203 - $15.00 USD Received 22 Sep 2011; revised 21 Oct 2011; accepted 28 Oct 2011; published 16 Nov 2011

"p" at the position *"k"* and t_{ch} is the inter chip separation. The spectral response then can be written as

$$H_p^{en}(\omega) = H_{chip}(\omega) \cdot \sum_{k=1}^{N} a_{p,k}^{en} \exp(j\phi_{p,k}^{en}) \exp(jk\omega t_{ch}) \tag{2}$$

where the $H_{chip}(\omega)$ is the global spectral envelope and corresponds to the Fourier transform of $h_{chip}(t)$. On the other hand, the complete summation term in (2) corresponds with a spectrally periodic function having a Frequency Repetition Period FRP = $1/t_{ch}$. The decoder is constructed by inscribing the reverse and conjugated code in its FBG structure. Thus, the exit global system response can expressed as the convolution of the two contributions

$$y_{p,q}(t) = x(t) \otimes h_{p,q}^{system}(t) = h_{pulses}(t) \otimes h_{p,q}^{coding}(t) \tag{3}$$

The term $h_{pulses}(t) = x(t) \otimes h_{chip}(t) \otimes h_{chip}(t)$ is the part related with the input pulse shape $x(t)$ and those of the encoder and the decoder, where for simplicity we have considered that the individual impulse responses of the encoder and the decoder are equal. The part corresponding to the coding is

$$h_{p,q}^{coding}(t) = \sum_{k=1}^{N} a_{p,k}^{en} \exp(j\phi_{p,k}^{en}) \delta(t - kt_{ch}) \otimes \sum_{l=1}^{N} a_{q,l}^{dec} \exp(j\phi_{q,l}^{dec}) \delta(t - lt_{ch}) \tag{4}$$

where $a_{q,l}^{dec}$ and $\phi_{q,l}^{dec}$ correspond to the code word *"q"* at the position *"l"* imposed by the decoder. At the receiver front end, it is typical to assume a time gating with duration T_g and, thus, only accomplishing time integration along the inter-chip time interval around the peak of the decoded signal. This requires high speed electronics and/or nonlinear optical processing making more complex and costly the final device. Nevertheless, the main advantage of time gating is that the multi user interference noise contribution appearing along the whole bit period is rejected. In our calculations, we consider the typical value $T_g = t_{ch}$. Therefore, the signal obtained at the receiver photodetector when the code pattern is decoded correctly ($p = q$) is proportional to the gated autocorrelation, which has the expression

$$acp_p = \frac{1}{T_g} \int_{-T_g/2}^{T_g/2} \left| y_{p,p}(t) \right|^2 dt \tag{5}$$

We define the averaged wings as the averaged contribution of the signal outside the temporal gate:

$$w_p = \frac{1}{T_{tot}} \left[\int_{-T_{tot}/2}^{-T_g/2} \left| y_{p,p}(t) \right|^2 dt + \int_{T_g/2}^{T_{tot}/2} \left| y_{p,p}(t) \right|^2 dt \right] \tag{6}$$

where T_{tot} is the signal total duration. The dimensionless gated autocorrelation to wings ratio of code *"p"* is acp_p/w_p. A single value that informs about the quality of the whole family of codes is the averaging over all the codes, that is

$$r_w = \frac{1}{M} \sum_{p=1}^{M} acp_p / w_p \tag{7}$$

where M is the number of used codes of the family. When the encoded signal is not correctly decoded a cross correlation signal is obtained. We consider that the contribution of this signal to the noise figure must be time averaged because the encoded signal *"p"* is asynchronous to the decoding receiver *"q"*, consequently the cross correlation must be time independent. Thus, the averaged cross correlation term is

$$c_{p,q} = \frac{1}{T_{tot}} \int_{-T_{tot}/2}^{T_{tot}/2} \left| y_{p,q}(t) \right|^2 dt \tag{8}$$

#155203 - $15.00 USD Received 22 Sep 2011; revised 21 Oct 2011; accepted 28 Oct 2011; published 16 Nov 2011

Hence, the dimensionless autocorrelation to cross correlation gated ratio *(A/C)* for the case where the encoded signal with code *"p"* is decoded with the pattern *"q"* is $acp_p/c_{p,q}$. The quality of the global system is calculated averaging *(A/C)* over all the possible code combinations, obtaining a gated ratio of the form

$$r_g = \frac{1}{M(M-1)} \sum_{p=1}^{M} \sum_{q \neq p}^{M} acp_p / c_{p,q} \tag{9}$$

The quality of the en/decoding process depends on the shape and width of the h_{pulses} function. This function is the result of a double convolution, thus we can consider h_{pulses} as a Gaussian function with temporal width σ_t [9], or equivalently a bandwidth $\sigma_f = 1/(2\pi\sigma_t)$. Figure 1 shows the evolution of the averaged gated ratio r_g and the gated autocorrelation to wings ratio r_w in function of the full width half maximum (FWHM) frequency bandwidth for a family of M = 32 gold codes with length N = 63. In the simulations we have considered that the gate width is equal to the inter-chip separation t_{ch}. We employ in Fig. 1 the dimensionless ratio FWHM/FRP that is directly related to the ratio between system chip width and inter-chip separation t_{ch}/σ_t

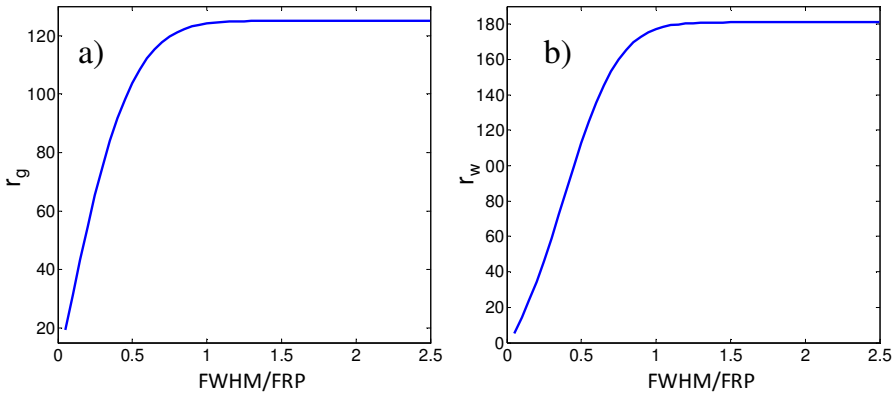

Fig. 1. Averaged gated ratio r_g, a). Averaged *acp/w*, r_w ratio b)

We observe that both the averaged autocorrelation to cross correlation gated ratio (r_g) and the gated autocorrelation to wings ratio (r_w) attain a maximum value when the pulses function bandwidth is around *FRP*. Thus, for a system with high coding capacity, the compound signal $h_{pulses}(t) = x(t) \otimes h_{chip}(t) \otimes h_{chip}(t)$ must have a bandwidth at least of the order of *FRP*. Therefore, it is possible to allocate several WDM frequency channels (*S* channels) and encode them with a single device without coding capacity loss, if the en/decoder global spectral envelope $H_{chip}(\omega)$ does not present notches in a bandwidth of the order of *S·FRP*. In the system presented in [8] they encode three channels sharing a single FRP with FRP/3 channel separation and thus it is not optimal in terms of coding capacity.

In a real situation, the non-limited spectral response of the ideal component, whose impulse response is $h_{i,j}^{coding}(t)$ (4), is reduced by the frequency response of the individual technological elements that accomplish the en/decoding process hchip(t). The most employed technology consists in the use of SSFBG structures that provide a local and distributed reflectivity along the whole inter-chip separation (tch). In this case, the device global spectral envelope Hchip(ω) corresponds to a sinc-like function with main lobe FWHM bandwidth approximately equal to *0.9·FRP* and strong notches at ± *FRP*. Consequently, due to the presence of the notches, in the standard scheme it is only possible to encode a code in the main lobe without coding capacity loss. Hence, in order to increase the SSFBG bandwidth, we propose an SSFBG in which the information of each chip is only inscribed in a narrow region of the fiber during the fabrication process, giving rise to a device whose bandwidth is independent of the inter-chip separation (t_{ch}). This aspect of SSFBGs has not been addressed

#155203 - $15.00 USD Received 22 Sep 2011; revised 21 Oct 2011; accepted 28 Oct 2011; published 16 Nov 2011

in the literature but it has an important impact on the frequency range over the SSFBG en/decoders. Figure 2 shows an illustrative simulation for a 17 chip code length and summarizes two representative cases for t_{ch} = 10ps: 1) Standard square shape chip covering the whole inter-chip separation. In this case the spectral envelope is a sinc-like function with notches at ± FRP (FRP = 100GHz) where we can only employ the narrow central lobe. 2) Here, we propose a Gaussian chip with reduced chip temporal width ($\sigma_{chip,t}$) of 1ps which provides a broadband spectral envelope without notches. We can see that, in addition to the central band, the lateral bands at ± FRP and ± 2FRP can be employed for the encoding of the same code information simultaneously for different transmitters on a single device. The only drawback in using multiband SSFBG encoders is the different power loss caused by the shape of the global spectral envelope. The fast variation pattern in Fig. 2 is determined by the summation term containing the code information in (2).

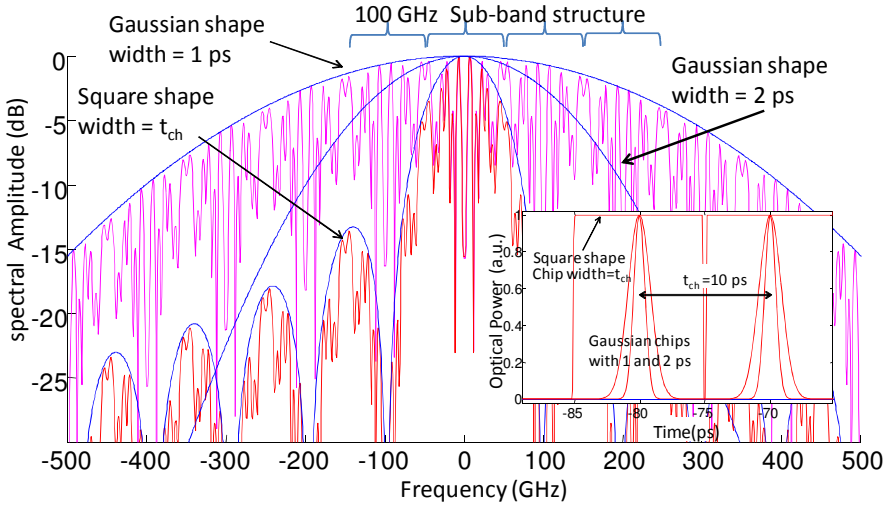

Fig. 2. Multi-Band proposal by shortening the chip temporal width $\sigma_{chip,t}$. Inset: Chip temporal shapes.

2. Multi-band SSFBG fabrication process

The fabrication technique used by our group consist in focusing a ultraviolet laser argon–ion laser emitting at 244 nm into a boron–germanium codoped photosensitive single-mode fiber by means of the phase mask technique. During the fabrication process the optical fiber remains in a fixed position while the phase mask and the UV beam displace along the optical axis with the aid of a controlled translation stage so as to provide accurate Bragg phase control. Please note that the phase coding is done by controlling the position of the illuminations, and then the same uniform phase mask can be used to inscribe all the code patterns of the different Multiband SSFBGs. The illumination is only done in some specific regions of the fiber core, in the so called chip by chip illumination technique. The chip by chip inscription is achieved with the aid of an optical shutter placed at the exit of the UV laser. In the exposed areas, the process is accomplished at constant UV power and exposition time to avoid induced chirp. Normally, SSFBGs are fabricated in the low reflectivity regime, so the illumination figure during the fabrication process is mapped on the impulse response. Thus, to obtain a device with a bandwidth much greater than the FRP each chip has to be only inscribed in a narrow region of the fiber during the fabrication process. Therefore, we have reduced the ultraviolet laser beam width σ_{UV} during the fabrication process by means of a convergent lens placed in between the UV laser and the phase mask. If we consider the illumination beam as Gaussian with σ_{UV} width, the individual chip impulse $h_{chip}(t)$ will be also

#155203 - $15.00 USD Received 22 Sep 2011; revised 21 Oct 2011; accepted 28 Oct 2011; published 16 Nov 2011

Gaussian with width $\sigma_{chip,t} = (2n/c)\cdot\sigma_{UV}$, where n is the fiber core refractive index and c the speed of light. The global envelope will also have a Gaussian shape with a width

$$\sigma_{chip,\omega} = \frac{c}{2n\sigma_{UV}} \tag{10}$$

this relationship allows us to control the encoder bandwidth independently of the chip rate ($1/t_{ch}$).

In Fig. 3 we can see the effect of the focused UV on the frequency response. We have fabricated a 63 long code with L_{ch} = 1 mm (FRP = 100 GHz) in the low reflectivity regime.

In the case where the laser pulse is not further focalized, we obtain a global envelope of the order of FRP. On the other hand, for the focused beam setup we set $\sigma_{UV} = 100\mu m$ and we obtain a much wider spectrum with a FWHM of approximately 300 GHz.

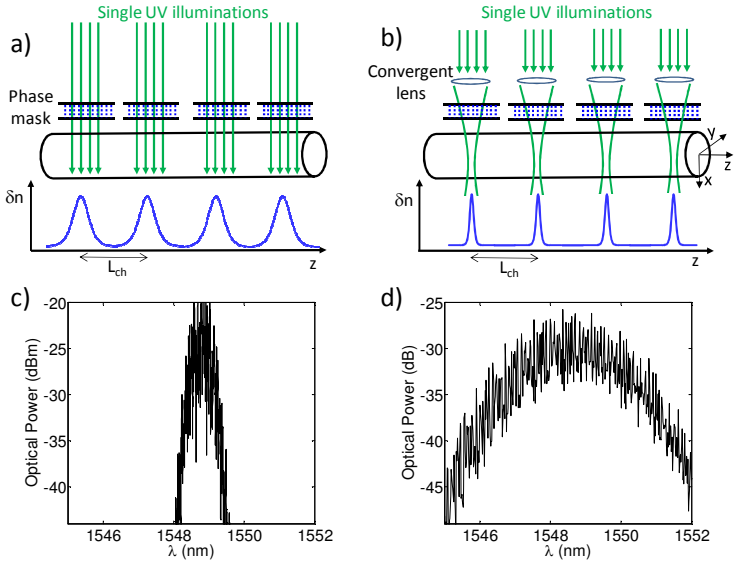

Fig. 3. Comparison between the non focalized fabrication and the proposed focalized UV beam technique in the low reflectivity regime. Scheme of the standard not focalized technique a). Scheme of the chip by chip with focalizing lens b). Measured spectrum for non focalized c) and focalized technique d)

3. Multi-band en/decoding experimental verification

In this section we demonstrate the multi-band (MB) en/decoding operation by using two codes and four WDM channels (CH1 to CH4). Seven MB_SSFBG en/decoders (2 encoders and 5 decoders) with 63 chips encoded by means of binary phase changes were fabricated. For the chip by chip fabrication, we used a focused Gaussian UV fringe pattern (σ_{UV} = $100\mu m$) to produce a short chip width compared to the inter-chip separation that was fixed to 1 mm (t_{ch} = $10ps$) to provide 100 GHz ITU sub-band channelling. The final en/decoding devices present 4x100GHz sub-bands with an insertion loss penalty between 3 and 4 dB from centre to lateral bands, allowing us to encode four 100 GHz channels without requirements of WDM devices.

Figure 4 shows the system set up for the multiband en/decoding. The two encoders are labeled C1 and C2 respectively for code "1" and code "2". We employed four optical sources at 1.25 Gp/s: three DFB lasers (CH2, CH3, CH4) pulsed by gain switching technique [10] coded with encoder C1 and a Tunable Mode Locked Laser (MLL). The MLL source can be tuned alternatively between CH1 to CH4 and codified with both codes. At the receiver front end, for the demultiplexing stage, we employed four adjacent channels of an Array

#155203 - $15.00 USD Received 22 Sep 2011; revised 21 Oct 2011; accepted 28 Oct 2011; published 16 Nov 2011

Waveguide Grating (AWG) router with 0.8 nm channel spacing and 0.4 nm 3 dB bandwidth. After channel filtering, we used four identical MB_SSFBG to decode code 1 C1c (A to D) and one MB_SSFBG to decode code 2: C2c. In this case we only used one sub-band at each decoder because the signal to each remote node comes from the AWG. Nevertheless, in general network scenery the multiple band decoders could be exploited in different way with no band limitation for the decoding device. The seven MB-SSFBG were fed through the respective circulators and placed into thermal boxes to compensate their detuning after fabrication and to ensure a stable operation. Please note that there is only one SSFBG needed per code pattern on the encoder side and then only one thermal box is required in contrast with the previous proposals [5], [7] where for each sub-band and each code a SSFBG a thermal box is necessary making the system more complex and cumbersome.

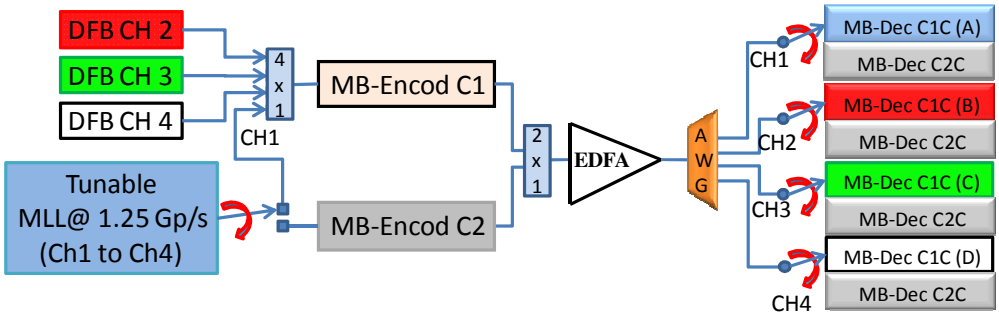

Fig. 4. Experimental system set-up.

Figure 5(a) shows the spectra for en/decoders implementing code 1. The traces have been displaced vertically for better representation. We can clearly identify the spectral repetition period of 100GHz (0.8 nm) and the slow decaying envelope lower than 2 dB at 0.8 nm from maximum and 4 dB for 1.6 nm. We can observe slight differences on the spectral shapes due to inaccuracies produced in the fabrication process. For example, fiber and mask separation must be adjusted to ~60 μm and maintained along the device (6.3 cm). Also constant mechanical strain is applied to the fiber to minimize the bending which affects the spectral response. In addition, an electronic UV beam electronic tracking is employed to follow the minor fiber tilt for long gratings.

Note that the obtained broadband spectral envelope can be employed for coding a single very broad band pulsed signal (like in a standard approach), or divided in sub-bands, as we propose here, in a WDM-OCDMA system employing narrower optical sources. It is important to note that there is no constraint of the WDM channels allocation with regard to the spectral shape of the en/decoders. Therefore, the channels central frequency can be freely chosen providing an additional degree of freedom for the system design. Figure 5(b) provides a more precise measurement of the Multi-Band en/decoders along 2.5 nm wavelength span with detail of the AWG bands used in the WDM demultiplexing. We can see the fast spectral periodic profile and the perfect matching between the encoder and the decoder to perform the ACP recovery by means of the thermal control. This strict wavelength matching for ACP recovery between C1 and C1c can be relaxed between different codes (C1 and C2) without increasing the interfering cross-correlation signal [11]. In the case of the proposed multiband encoders this circumstance can be easily exploited due to the broad bandwidth without notches at the envelope.

#155203 - $15.00 USD Received 22 Sep 2011; revised 21 Oct 2011; accepted 28 Oct 2011; published 16 Nov 2011

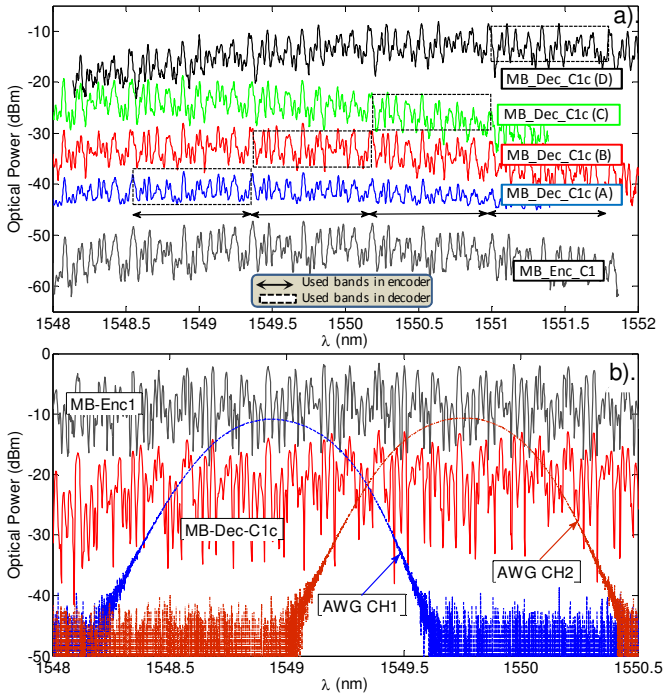

Fig. 5. a) Spectral measurement of the Multi-band en/decoders, b) Spectrum detail with respect to the AWG bands.

Figure 6 shows the spectra captured at the AWG outputs of the DFBs signals encoded with the MB_SSFBG C1 and the MLL signal codified with code 2 and tuned to CH1. We can see the same spectra shape for channels CH2, CH3 and CH4, which corresponds to C1 and a different shape for CH1 which has been codified using C2. We observe that each WDM channel covers a different portion of the MB_SSFBG spectrum. We can also see that the inter-channel crosstalk level is lower than 20 dB for all channels avoiding any possible interference effect on the quality of the codification. This principle can be replicated for a higher number of sub-bands being affected by additional insertion losses given by the slow decaying envelope of the multi-band encoder. After codification the aggregate of signals can be transmitted through the link; finally, they can be redirected to different optical remote nodes by WDM demultiplexing, such as WDM Passive Optical Network (PON) architecture.

#155203 - $15.00 USD Received 22 Sep 2011; revised 21 Oct 2011; accepted 28 Oct 2011; published 16 Nov 2011

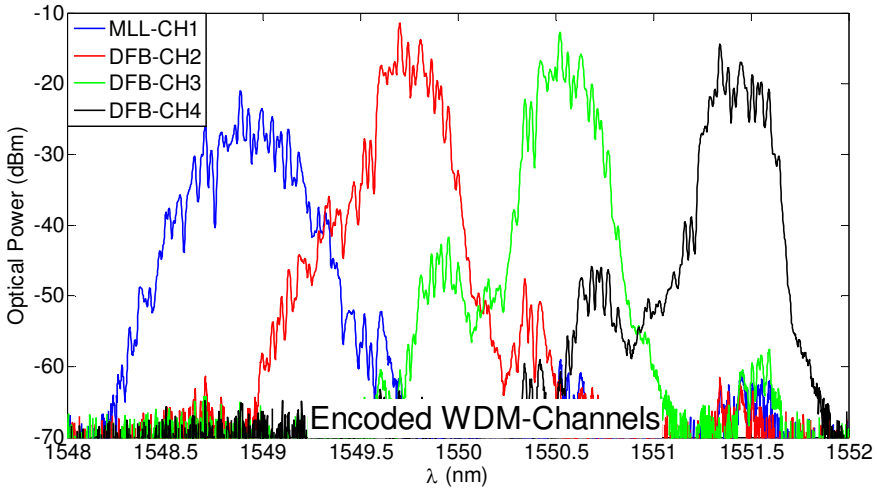

Fig. 6. Encoded spectrums at the AWG outputs. Code 2 in CH1 (blue), Code 1 in CH2 (red), CH3 (green) and CH4 (black)

Figure 7 shows the transmitted encoded sequences when each source was switched on independently. Notice how the MB_SSFBG C1 encoder provides an identical encoded sequence for the pulses centered at wavelength of CH2 and CH3. CH4 is not shown in Fig. 7 but it has also the same shape as CH2 and CH3 since it is codified using the same MB_SSFBG encoder. We can also observe that all encoded signals present strong amplitude variations which should not be present in bipolar phase encoding. This effect is due to the interference between adjacent chips with 0 to π phase change (or vice versa) and is caused by the higher pulse width than inter-chip separation of the available optical sources for the experiment. For the DFB input pulse width is around 45 ps and for the MLL is around 25 ps. This figure is also limited by the sampling oscilloscope electrical bandwidth (80 GHz). In any case this is a practical limitation on the experimental demonstration and it does not affect conceptually to the multi-band en/decoding concept.

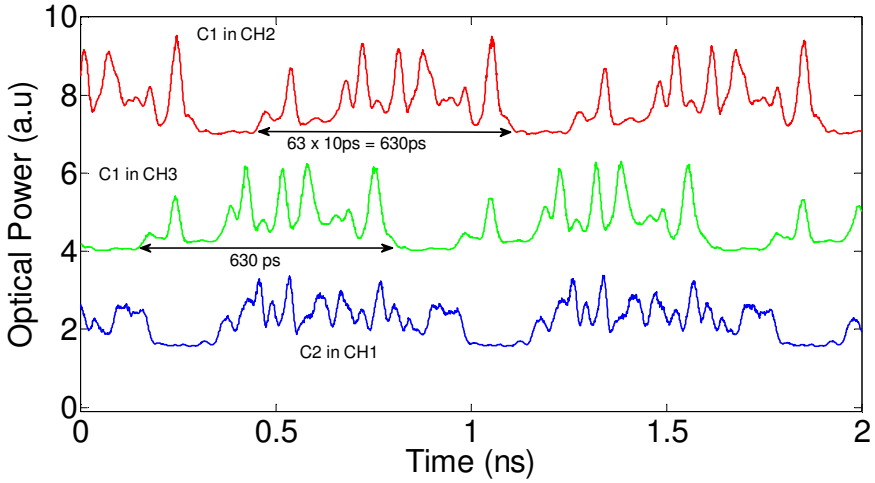

Fig. 7. Codified sequences at the AWG input. Code 2 in CH1 (blue), Code 1 in CH2 (red) and CH3 (green)

The WDM-OCDMA en/decoding process was verified by the pulsed signal recovery (Fig. 8) at the exit of each decoder. We observe a sharp Auto-Correlation Peak (ACP) for the matched pairs (C1*C1c and C2*C2c for each channel) and a noise-like Cross-Correlation

#155203 - $15.00 USD Received 22 Sep 2011; revised 21 Oct 2011; accepted 28 Oct 2011; published 16 Nov 2011

(XC) (C1*C2C and C2*C1c for each channel). ACP power was adjusted to the same value for all cases to perform the ACP/XC ratio in the same interfering conditions and it was about 10 dB for the worst case. Higher effective ACP/XC ration should be expected for a 63 chip bipolar code but in our experimental setup it was limited by the DFBs and MLL pulse widths and also by the sampling oscilloscope electrical bandwidth.

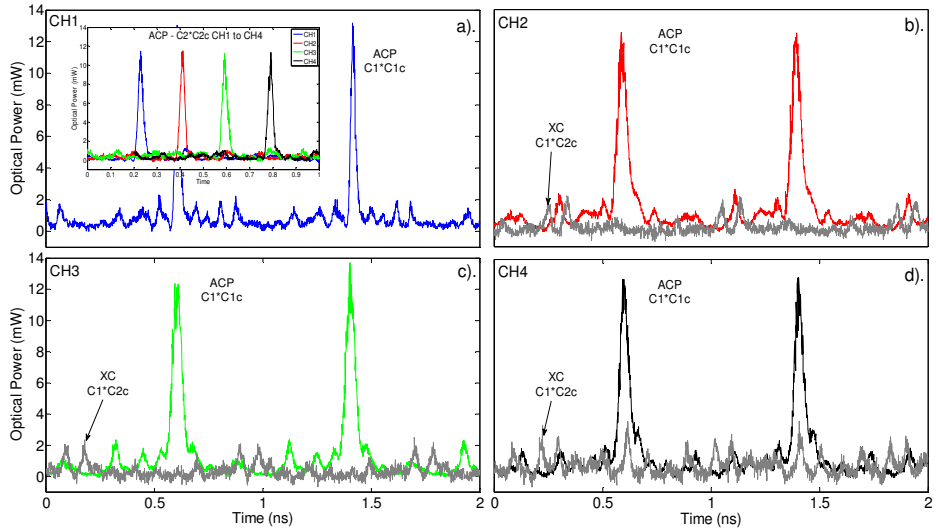

Fig. 8. Decoded temporal signals at the exit of each decoder when the code is correctly decoded and when the encoder and decoder patterns do not match. Inset autocorrelation figures for C2*C2c case using the MLL.

We must point out some optical network considerations which are closely related to the features and required number of the en/decoding devices. In optical access networks with WDM signal distribution such as the one proposed in the experimental set-up, each Optical Network Unit (ONU) is situated in a different location. Each ONU receives a single channel (encoded sub-band) with fix spectral location for the case of static optical networks or even with tunable spectral location for reconfigurable optical networks. In this situation MB-SSFBG decoders provide decoding capabilities for a given number of sub-bands on the same device. Moreover, the optical network described could be extended to support more than one sub-band could reach simultaneously the ONUs. In this case, the MB-SSFBG decoder maintains its features decoding simultaneously each sub-band but a wavelength demultiplexing device (i.e AWG or FBGs) must be employed after the MB-SSFBG decoder. Finally, standard SSFBG decoders covering just only one band could be employed to decode signals from MB-SSFBG encoders with no need of wavelength demultiplexing. However, the upgrade of the network will require new devices including their independent thermal control, increasing complexity and cost.

3. Conclusion

We have proposed, fabricated and demonstrated experimentally a multi-channel broadband Coherent Direct Sequence en/decoder for WDM-OCDMA applications. The device operation is based on SSFBGs with short chips compared with its device chip separation. The obtained device presents a broadband envelope with respect to its periodic spectral pattern that can be employed for en/decoding of multiple sub-bands simultaneously. For the experimental verification we fabricated Super Structured Fiber Bragg Gratings with 63 chips encoded in binary phase with 1mm inter-chip separation that provides 100 GHz ITU sub-band channeling. The final en/decoding device presents up to 4x100GHz sub-bands with an insertion loss penalty between 3 and 4 dB from centre to lateral bands.

#155203 - $15.00 USD Received 22 Sep 2011; revised 21 Oct 2011; accepted 28 Oct 2011; published 16 Nov 2011

Acknowledgments

We would like to thank our reviewers for their thoughtful comments and suggestions. This work was supported by the Spanish Government project TEC 2009-12169, and the Valencian Government under the project ACOMP/2010/023.

#155203 - $15.00 USD Received 22 Sep 2011; revised 21 Oct 2011; accepted 28 Oct 2011; published 16 Nov 2011